THE JOURNAL OF BIOLOGICAL CHEMISTRY
Vol. 277, No. 34, Issue of August 23, pp. 30852–30858, 2002

Printed in U.S.A.

Fast and Slow Inactivation Kinetics of the Ca^{2+} Channels ECaC1 and ECaC2 (TRPV5 and TRPV6)

ROLE OF THE INTRACELLULAR LOOP LOCATED BETWEEN TRANSMEMBRANE SEGMENTS 2 AND 3*

Received for publication, March 13, 2002, and in revised form, March 15, 2002
Published, JBC Papers in Press, June 19, 2002, DOI 10.1074/jbc.M202418200

Bernd Nilius‡§, Jean Prenen‡, Joost G. J. Hoenderop¶, Rudi Vennekens‡, Susan Hoefs¶, A. Freek Weidema¶, Guy Droogmans‡, and René J. M. Bindels¶

From the ‡Department of Physiology, Campus Gasthuisberg, B-3000 KU Leuven, Belgium and ¶Department of Cell Physiology, Nijmegen Centre for Molecular Life Sciences, University Medical Centre, 6500 Nijmegen, The Netherlands

The Ca^{2+} channels ECaC1 and ECaC2 (TRPV5 and TRPV6) share several functional properties including permeation profile and Ca^{2+}-dependent inactivation. However, the kinetics of ECaC2 currents notably differ from ECaC1 currents. The initial inactivation is much faster in ECaC2 than in ECaC1, and the kinetic differences between Ca^{2+} and Ba^{2+} currents are more pronounced for ECaC2 than ECaC1. Here, we identify the structural determinants for these functional differences. Chimeric proteins were expressed heterologously in HEK 293 cells and studied by patch clamp analysis. Both channels retained their phenotype after exchanging the complete N termini, the C termini, or even both N and C termini, *i.e.* ECaC1 with the ECaC2 N or C terminus still showed the ECaC1 phenotype and *vice versa*. The substitution of the intracellular loop between the transmembrane domains 2 and 3 of ECaC2 with that of ECaC1 induced a delay of inactivation. Three amino acid residues (Leu-409, Val-411 and Thr-412) present in this loop determine the fast inactivation behavior. When this intracellular loop between the transmembrane domains 2 and 3 of ECaC1 was exchanged with the TM2-TM3 loop of ECaC2, the ECaC1 kinetics were analogous to ECaC2. In conclusion, the TM2-TM3 loop is a critical determinant of the inactivation in ECaC1 and ECaC2.

Ca^{2+} entry channels play a pivotal role in the regulation of cell functions such as contraction, secretion, gene expression, molecular transduction of painful stimuli, osmoregulation, and transepithelial ion transport. The advent of a novel superfamily of cation channels, the TRP[1] family, made it possible to investigate novel Ca^{2+} entry pathways at the molecular level in a plethora of cells (1). Most of the channels cloned and characterized so far from the TRPC subfamily and also the vanilloid receptors TRPV1, TRPV2, and TRPV4 have only a moderate selectivity for Ca^{2+} over monovalent cations. Functional characterization of the recently cloned ECaC subfamily of cation channels (2, 3) revealed a pore structure with a high selectivity for Ca^{2+} (4). This subfamily is restricted to two homologous members, namely ECaC1 and ECaC2 (previously named calcium transporter 1 (CaT1)). These novel Ca^{2+} channels are implicated in hormonal-regulated active Ca^{2+} transport in epithelia-like kidney and small intestine. Both channels consist of six transmembrane-spanning domains including a putative pore-forming region between transmembrane segments 5 and 6. Genomic analysis shows that ECaC1 and ECaC2 originate from two genes juxtaposed on human chromosome 7q35 and mouse chromosome 6 (5–7).

We have recently described that ECaC1 and ECaC2 share several functional properties but also functional differences (8, 9). When heterologously expressed in human embryonic kidney (HEK) 293 cells, both ECaC members function as highly Ca^{2+}-selective channels that are constitutively open (10–13). Both channels have the same Eisenman X permeation sequence for monovalent cations, the same single channel conductance in the absence of extracellular divalent cations, and display anomalous mole fraction behavior. Monovalent cation currents through ECaC are blocked by extracellular Mg^{2+} with an IC_{50} of 200 μM (−80 mV) and by extracellular Ca^{2+} with an IC_{50} between 0.2 and 2 μM (−80 mV) (10, 13, 14). Recently, it was demonstrated that also intracellular Mg^{2+} blocks both channels in a voltage-dependent manner (15). ECaC1 and ECaC2 are inhibited by intracellular Ca^{2+}, $[Ca^{2+}]_i$, with an IC_{50} of 200 nM (8, 11). Ruthenium Red is so far the most potent blocker of both channels; however, ECaC1 is significantly more sensitive compared with ECaC2 with IC_{50} values of 120 nM and 9 μM, respectively (8, 16).

Interestingly, there are essential differences between ECaC1 and ECaC2. ECaC1 and ECaC2 show in the presence of extracellular Ca^{2+} a fast initial inactivation at negative membrane potentials. However, this inactivation is much slower for ECaC1 (8) in comparison with ECaC2. Also with Ba^{2+} as the charge carrier, ECaC2 inactivates much slower and more complete than ECaC1 (8). This last feature is the most pronounced kinetic difference between ECaC1 and ECaC2.

The aim of the present study was to gain insight into the structural determination of ECaC1 and ECaC2, which are responsible for the differences in channel kinetics. To this end, chimeras were constructed from N and C termini and intracellular loops of these channels heterologously expressed in HEK 293 cells and subsequently studied by patch clamp analysis.

* This work was supported in part by the Belgian Federal Government (Interuniversity Poles of Attraction Program, Prime Minister's Office), the Flemish Government Grants GOA 99/07, F.W.O. G.0237.95, F.W.O. G.0214.99, F.W.O., and G.0136.00, Grant R71 from the "Alphonse and Jean Forton-Koning Boudewijn Stichting" (to B. N.), and the Dutch Organization of Scientific Research Grants Zon-mw 016.006.001 and NWO-ALW 810.38.004. The costs of publication of this article were defrayed in part by the payment of page charges. This article must therefore be hereby marked "*advertisement*" in accordance with 18 U.S.C. Section 1734 solely to indicate this fact.

§ To whom correspondence should be addressed: Campus Gasthuisberg, Laboratorium voor Fysiologie, Herestraat 49, B-3000 KU Leuven, Belgium. Tel.: 32-16-345937; Fax: 32-16-345991; E-mail: bernd.nilius@med.kuleuven.ac.be.

[1] The abbreviations used are: TRP, transient receptor potential; CaT1, calcium transporter 1; HEK, human embryonic kidney; TM, transmembrane; GFP, green fluorescent protein; N1 or N2, N-terminal tail of ECaC1 or ECaC2; C1 or C2; C-terminal tail of ECaC1 or ECaC2; ICL, intracellular linker; ANOVA, analysis of variance; NMDG, *N*-methyl-D-glucamine.

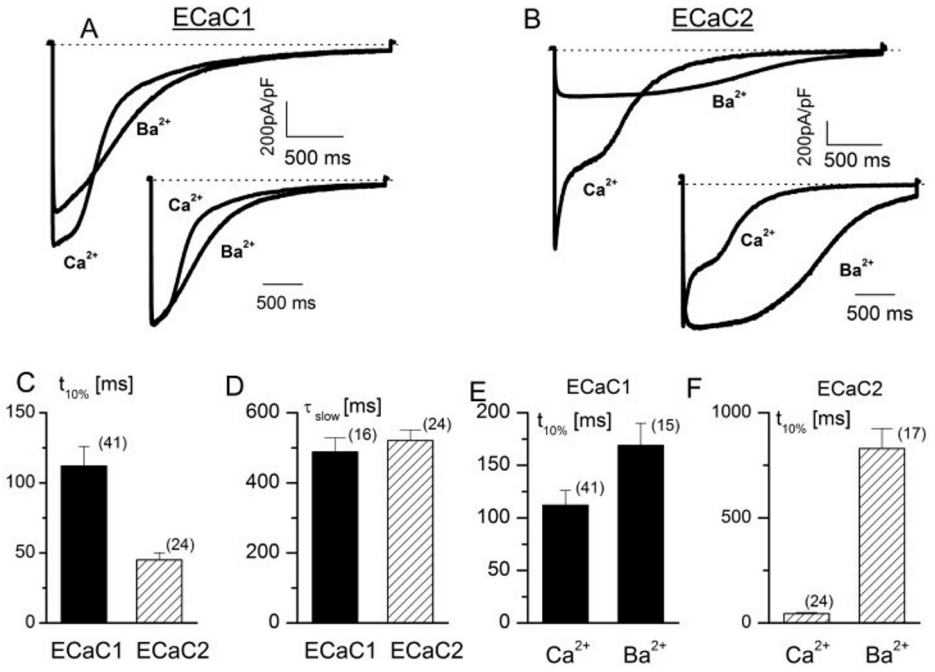

FIG. 1. **Inactivation of ECaC1 and ECaC2 currents in 30 mM $[Ca^{2+}]_e$.** *A* and *B*, currents through ECaC1 and ECaC2 in response to a voltage step to −100 mV (V_H = +70 mV) in the presence of 30 mM $[Ca^{2+}]_e$. All of the other cations are substituted by 150 mM NMDG. Cells were loaded with 10 mM BAPTA. The *insets* show currents normalized to the peak. *C*, pooled data comparing the time for 10% inactivation ($t_{10\%}$) during a voltage step as in *A* and *B* between ECaC1 and ECaC2. The number of cells is indicated in *parentheses*. *D*, pooled data comparing the time constants of the monoexponential fit of the last 1.5 s of the voltage step as in *A* and *B* ($\tau_{1.5s}$) between ECaC1 and ECaC2. *E*, the time to 10% decay for Ba^{2+} and Ca^{2+} currents through ECaC1. *F*, same as in *E* but through ECaC2.

Surprisingly, the N and C termini of both channels are not responsible for the distinctive kinetic differences between ECaC1 and ECaC2. However, we identified a region in the intracellular linker between transmembrane domains 2 and 3 (TM2 and TM3) that determines the initial current decay and the degree of inactivation.

MATERIALS AND METHODS

Construction of Mammalian Expression Vectors—The entire open reading frame from mouse ECaC2/CaT1 was cloned as a *Eco*RI fragment from pSPORT-mECaC2 in the pCINeo/IRES-GFP vector. This bicistronic expression vector pCINeo/IRES-GFP/ECaC2 was used to co-express ECaC2 and green fluorescent protein (GFP). The entire open reading frame from rbECaC1 was cloned as a *Pvu*II-*Bam*HI fragment in the pCINeo/IRES-GFP vector as described previously (12). To exchange the ECaC1 N terminus for the ECaC2 N terminus, a unique *Bsp*EI site has been incorporated at amino acid position Ser^{221}-Tyr^{222} without affecting the amino acid composition. The N terminus of ECaC1 was cloned as a *Nhe*I-*Bsp*EI fragment into the ECaC2 expression vector, resulting in a chimeric transcript ECaC1-N2, and *vice versa* for ECaC2, resulting in ECaC2-N1. A similar strategy was applied to swap the C-terminal tails by introducing a unique *Bsi*WI site at amino acid position Arg^{615}-Ser^{616}. The *Nhe*I-*Bsi*WI fragments were exchanged, resulting in ECaC1-C2 and ECaC2-C1, respectively. Subsequently, using the introduced restriction sites, chimeric transcripts were constructed containing the ECaC1 core protein with the N- and C-terminal tail of ECaC2 (ECaC1-N2C2) and the ECaC2 core protein with the N- and C-terminal tail of ECaC1 (ECaC2-N1C1). Finally, the four discriminating amino acids in the intracellular loop between TM2 and TM3 of ECaC2 (L409V, V411A, T412S, and F414Y) were mutated according to the ECaC1 sequence and *vice versa* by site-directed mutagenesis as described previously (12). All of the constructed transcripts were verified by sequence analysis.

Cell Culture and Transfection—HEK 293 were grown in Dulbecco's modified Eagle's medium containing 10% (v/v) human serum, 2 mM L-glutamine, 2 units/ml penicillin, and 2 mg/ml streptomycin at 37 °C in a humidity-controlled incubator with 10% (v/v) CO_2. HEK 293 cells were transiently transfected with the pCINeo/IRES-GFP/rbECaC1 or pCINeo/IRES-GFP/mECaC2 vector using methods as described previously (12). Transfected cells were visually identified in the patch clamp setup. GFP was excited at a wavelength between 425 and 475 nm. A 495-nm dichroic mirror was used for GFP, and the emitted light was passed through a 500-nm long pass filter for GFP. The ECaC1/ECaC2-expressing cells were identified by their green fluorescence, and GFP-negative cells from the same batch of cells were used as controls.

Electrophysiology—Electrophysiological methods have been described previously in detail (11, 12). Whole-cell currents were measured with an EPC-9 (sampling rate 0.2 ms, 8-pole Bessel filter 10 kHz, HEKA Elektronik, Lambrecht, Germany) or an L/M-EPC-7 (List Elektronics, Darmstadt, Germany) using ruptured patches. Electrode resistances were between 2 and 5 megohms, and capacitance and access resistance were monitored continuously. A ramp protocol consisting of linear voltage ramps changing from −100 to +100 mV within 400 ms was applied every 5 s. To study inactivation and the much slower current decay with Ca^{2+} as the charge carrier in a single protocol, we have applied 3-s voltage steps to −100 mV from a holding potential of +20 or +70 mV. Fast inactivation was assessed by the time for 10% decay of the current, the slower run down by the time constant of a monoexponential fit to the current during the last 1.5 s of the step. Current densities expressed per unit membrane capacitance were calculated from the current at −80 mV during the ramp protocols.

Solutions and Experimental Procedures—The standard extracellular solution (Krebs-Ringer phosphate solution) contained (in mM) 150 NaCl, 6 CsCl, 1 $MgCl_2$, 10 HEPES, and 10 glucose, pH 7.4, adjusted with CsOH. The concentration of Ca^{2+}, Ba^{2+}, Sr^{2+}, or Mn^{2+} was varied between 1 and 30 mM as indicated in the text. Nominally free Ca^{2+} concentration was estimated at 10 μM. Ca^{2+}-free solutions were buffered by 5 mM EGTA at a free $[Ca^{2+}]$ below 1 nM as calculated by the CaBuf program (G. Droogmans, ftp.cc.kuleuven.ac.be/pub/droogmans/cabuf.zip). To inhibit monovalent cation currents, 150 mM NaCl was replaced with an equimolar amount of NMDG-Cl. The standard internal (pipette) solution contained (in mM) 20 CsCl, 100 Cs-aspartate, 1 $MgCl_2$, 10 BAPTA, 4 Na_2ATP, and 10 HEPES, pH 7.2, adjusted with CsOH. Cells were kept in a nominally Ca^{2+}-free medium to prevent Ca^{2+} overload and exposed for maximum of 5 min to a Krebs-Ringer phosphate solution containing 1.5 mM Ca^{2+} before sealing the patch pipette to the cell. All of the experiments were performed at room temperature (20–22 °C).

Statistical Analysis—Data are expressed as the mean ± S.E. Overall statistical significance was determined by analysis of variance (ANOVA). In the case of significance ($p < 0.01$), individual groups were compared by Student's *t* test. Experimental data were fitted to a monoexponential function using the fitting routine of the WinASCD program (G. Droogmans). Dose-inhibition data were fitted to a dose response function using Origin software version 6.0 (Microcal Software, Northhampton, MA).

RESULTS

Kinetic Differences between ECaC1 and ECaC2 Currents—Inactivation of ECaC1 and ECaC2 currents with Ca^{2+} or Ba^{2+} as the charge carrier at negative potentials revealed the most striking functional difference between both channels. Fig. 1, *A* and *B*, shows representative current traces during a voltage step to −100 mV in solutions with all monovalent cations substituted by $NMDG^+$. Therefore, inward currents were car-

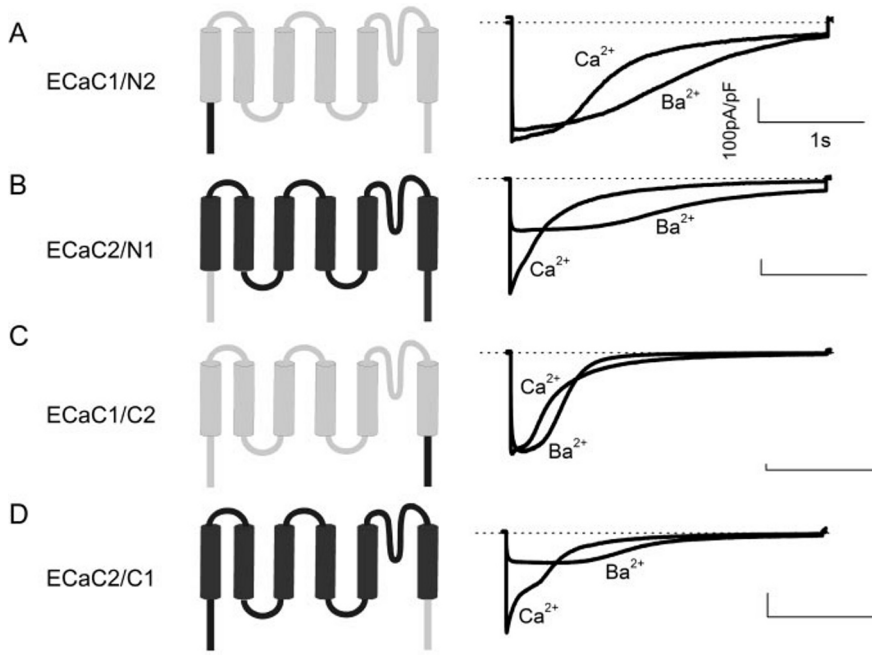

FIG. 2. **Changes in current pattern during hyperpolarizing voltage steps in ECaC1 and ECaC2 chimeras in which N and C termini were exchanged.** *A*, currents through the ECaC1-N2 chimera in which the N terminus of ECaC1 was exchanged with the N terminus of ECaC2. In all of the figures, *open* and *filled bars* represent structural components of ECaC1 and ECaC2, respectively. Current traces in response to a voltage step to −100 mV (V_H = +70 mV) in the presence of 30 mM $[Ca^{2+}]_e$ and all of the monovalent cations substituted by 150 mM NMDG. Cells were loaded with 10 mM BAPTA. *B*, currents through the ECaC2-N1 chimera in which the N terminus of ECaC2 was exchanged with the N terminus of ECaC1. Same protocol as in *A* was used. *C*, currents through the ECaC1-C2 (C terminus of ECaC1 exchanged with the C terminus of ECaC2). *D*, currents through the ECaC2-C1 (C terminus of ECaC2 exchanged with the C terminus of ECaC1).

ried by either Ca^{2+} or Ba^{2+}. The initial rapid phase of inactivation of ECaC2 assessed from the time to 10% current decay was significantly faster than that of ECaC1 (Fig. 1*C*). The late decay of the current assessed from the time constant of a monoexponential fit to the last 1.5 s of the voltage step to −100 mV was not significantly different between the two channels (Fig. 1*D*). If Ba^{2+} was used as the charge carrier, the time to 10% inactivation for ECaC1 was only modestly prolonged compared with the Ca^{2+} current (Fig. 1*E*). However, for ECaC2, these differences were significantly more pronounced (Fig. 1*F*) as is obvious from Fig. 1, *insets* in *A* and *B*, which shows the currents normalized to the peak values with Ca^{2+} as the charge carrier. Time to 10% inactivation was 112 ± 14 ms (n = 41) for Ca^{2+} currents through ECaC1 and 169 ± 21 ms (n = 15) for Ba^{2+} currents. The same measurements for ECaC2 resulted in 45 ± 5 ms (n = 24) for Ca^{2+} and 830 ± 95 ms (n = 17) for Ba^{2+}. The kinetic difference between both channels can be more impressively described by the ratio between these times, $t_{10\%,Ca}/t_{10\%,Ba}$, which was 0.66 for ECaC1 but 0.05 for ECaC2. The ratio of the Ca^{2+} and Ba^{2+} current densities was also significantly different between ECaC1 (0.69 ± 0.05 (n = 12)) and ECaC2 (0.39 ± 0.03 (n = 15)).

Exchange of the N and C Termini between ECaC1 and ECaC2—The N-terminal tails of ECaC1 (N1) and ECaC2 (N2), which share 81.3% homology, were exchanged to identify the structural determinants for the functional differences between these two channels. Fig. 2 shows typical traces of the inactivation of Ca^{2+} and Ba^{2+} currents for both chimeras. For ECaC1-N2, the chimera in which the ECaC1 N terminus was substituted by that of ECaC2, the time for 10% inactivation of the Ca^{2+} current remained long (210 ± 55 ms, n = 6) as is typical for ECaC1 (Fig. 2*A*) (see Fig. 4 for a summary of the analysis). In contrast, the time for 10% inactivation of the Ba^{2+} current was prolonged compared with that of wild-type ECaC1 (313 ± 79 ms, n = 6) but was still much shorter than that of ECaC2. The kinetic coefficient, $t_{10\%,Ca}/t_{10\%,Ba}$, was nearly identical to ECaC1. The ratio I_{Ba}/I_{Ca} was 1.03 ± 0.12 (n = 6, same cells). This ratio reflects the ECaC1 more than the ECaC2 phenotype. However, Ba^{2+} currents through this chimera were significantly larger compared with ECaC1.

The phenotype of ECaC2-N1 obtained by exchanging the N terminus of ECaC2 for that of ECaC1 was very similar to that of wild-type ECaC2. However, the decay of the Ba^{2+} current is significantly slower compared with the Ca^{2+} current (Fig. 2*B*). The time to 10% decay of the Ca^{2+} current was not significantly altered compared with wild-type ECaC2 (69 ± 11, n = 9), whereas the Ba^{2+} current is again prolonged (529 ± 136, n = 9). The ratio I_{Ba}/I_{Ca} was 0.45 ± 0.08 (n = 7, values only from the same cells) and not significantly different from wild-type ECaC2.

Because the exchange of the N-terminal tails did not affect the inactivation kinetics of the ECaC channel, we exchanged their C-terminal tails, which display a homology of 61%. It is obvious from the current traces in Fig. 2*C* that the time course of inactivation of the ECaC1-C2 chimera in which the ECaC1 C terminus is substituted by the complete C-terminal tail of ECaC2 is not significantly different from wild-type ECaC1 ($t_{10\%,Ca}$ = 230 ± 49, n = 9, and $t_{10\%,Ba}$ = 379 ± 66, n = 10). However, the ratio I_{Ba}/I_{Ca} was significantly increased to 1.15 ± 0.17 (n = 8) compared with wild-type ECaC1. Similarly, the kinetic properties of ECaC2-C1 obtained by replacing the ECaC2 C terminus with the C-terminal tail of ECaC1 were identical to those of wild-type ECaC2 (Fig. 2*D*). The time to 10% inactivation was 35 ± 7 ms (n = 11) for Ca^{2+} currents and 918 ± 112 ms (n = 12) for Ba^{2+} currents. Similarly, the I_{Ba}/I_{Ca} ratios were not significantly different, *i.e.* 0.43 ± 0.04 (n = 10) for ECaC2-C1 compared with 0.49 for the wild type.

In the next experiment, the effects of exchanging both N and C termini were studied. Fig. 3 summarizes the obtained results. The time to 10% inactivation of both Ca^{2+} and Ba^{2+} currents was significantly prolonged if ECaC1 contained both the N and the C termini of ECaC2 ($t_{10\%,Ca}$ = 512 ± 167 ms, n = 6, and $t_{10\%,Ba}$ = 825 ± 182 ms, n = 4). However, as for all chimeras, the differences between the kinetics of the Ca^{2+} and Ba^{2+} currents were small ($t_{10\%,Ca}/t_{10\%,Ba}$ = 0.62), and the fast initial phase of inactivation was lacking (Fig. 3, *A* and *B*). The I_{Ba}/I_{Ca} ratio of 1.06 ± 0.09 (n = 4, same cells) was increased but matched again the ECaC1 rather than the ECaC2 phenotypes. As for the other chimeras, the fast component of inactivation and the large differences in kinetics of the Ca^{2+} and Ba^{2+} currents were conserved whether the N- and the C-terminal tail of ECaC2 was exchanged with those of ECaC1 ($t_{10\%,Ca}$ = 94 ± 18 ms, n = 5, and $t_{10\%,Ca}/t_{10\%,Ba}$ = 678 ± 87 ms, n = 5) (Fig. 3, *C* and *D*). The ratio between the Ba^{2+} and Ca^{2+} cur-

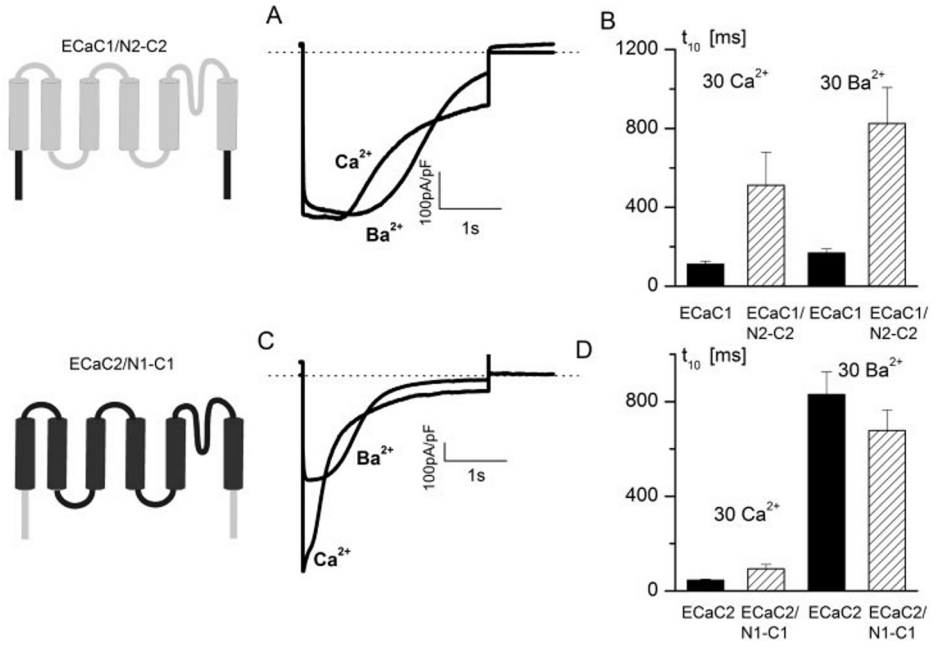

FIG. 3. **Inactivation properties of a chimera in which both N and C termini were exchanged for ECaC1 and ECaC2.** *A*, currents through the ECaC1-N2C2 chimera in which both the N terminus and C terminus of ECaC1 were exchanged by the ones of ECaC2. *B*, pooled data comparing the time for 10% inactivation ($t_{10\%}$) for wild-type ECaC1 and ECaC1-N2C2. *C*, currents through the ECaC2-N1C1 chimera in which the N and C termini of ECaC2 were exchanged with the tails of ECaC1. Same voltage protocol as in *panel A* was used. *D*, pooled data comparing the time for 10% inactivation ($t_{10\%}$) for wild-type ECaC2 and ECaC2-N1C1. Data are from 6 to 8 cells.

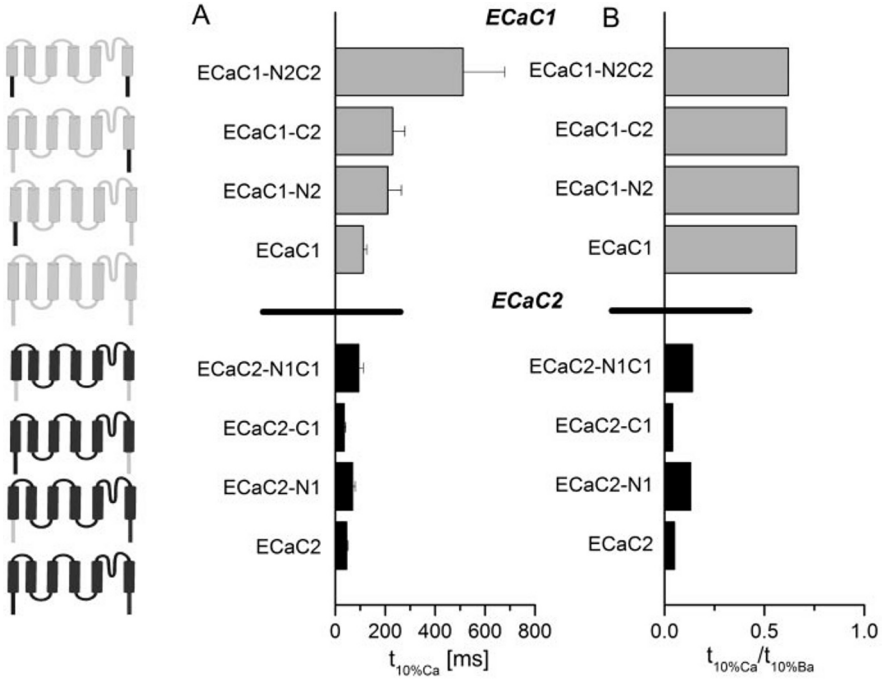

FIG. 4. **Summary of the fast decay by swapping of the N and C termini between ECaC1 and ECaC2.** *A*, the time to 10% inactivation with 30 mM Ca^{2+} as the charge carrier (data for ECaC1 shown on *top* and ECaC2 on *bottom*). All data are from between 4 and 41 cells. *B*, ratio of the time to 10% inactivation for Ca^{2+} and Ba^{2+} ($t_{10\%Ca}/t_{10\%Ba}$).

rents, I_{Ba}/I_{Ca}, was 0.56 ± 0.08 (n = 5, same cells) and similar to the ECaC2 phenotype. Both chimeras exhibit similar expression levels, *i.e.* the density of the monovalent cation current in the absence of divalent cations at −80 mV was −692 ± 46 pA/pF (n = 8) for ECaC1-N2C2 and −827 ± 114 pA/pF (n = 6) for ECaC2-N1C1.

Fig. 4 summarizes the data concerning the initial fast inactivation. The time to 10% decay of the Ca^{2+} current for all ECaC1 chimeras ranged between 100 and 500 ms. For ECaC2 and its chimeric proteins, the 10% current decay occurred in <100 ms (Fig. 4*A*). The initial decay of Ba^{2+} currents was slower than that of the Ca^{2+} currents. The ratio of the time to 10% decay of the Ca^{2+} current and the Ba^{2+} current ($t_{10\%,Ca}/t_{10\%,Ba}$) ranged between 0.5 and 0.9 for ECaC1 and its corresponding chimeras and was < 0.25 for ECaC2 and the corresponding chimeras.

The fraction of open channels at the end of a 3-s hyperpolarizing step expressed as the ratio of the current densities at the end of the pulse and the peak current was similar for all of the chimeras and for both charge carriers. This ratio, which scatters substantially and also depends on the size of the current (8), was <15% at the end of the pulse (Fig. 5), suggesting that the swapping of the N and C termini did not significantly affect the inactivation behavior. Therefore, the exchange of either or both N and C termini between ECaC1 and ECaC2 did not change severely the inactivation kinetics of the wild-type channel, indicating that other domains or even the core structure may determine the discriminating inactivation kinetics of ECaC1 and ECaC2.

Substitution of the Intracellular Linker Domain between the Transmembrane Regions TM2 and TM3—Because the exchange of the cytoplasmic N- and C-terminal tails did not affect the phenotype of the channel kinetics, we replaced the intracellular linker between TM2 and TM3 ($ICL1_{ECac1}$ for the ECaC1 linker and $ICL1_{ECaC2}$ for the ECaC2 linker). Intrigu-

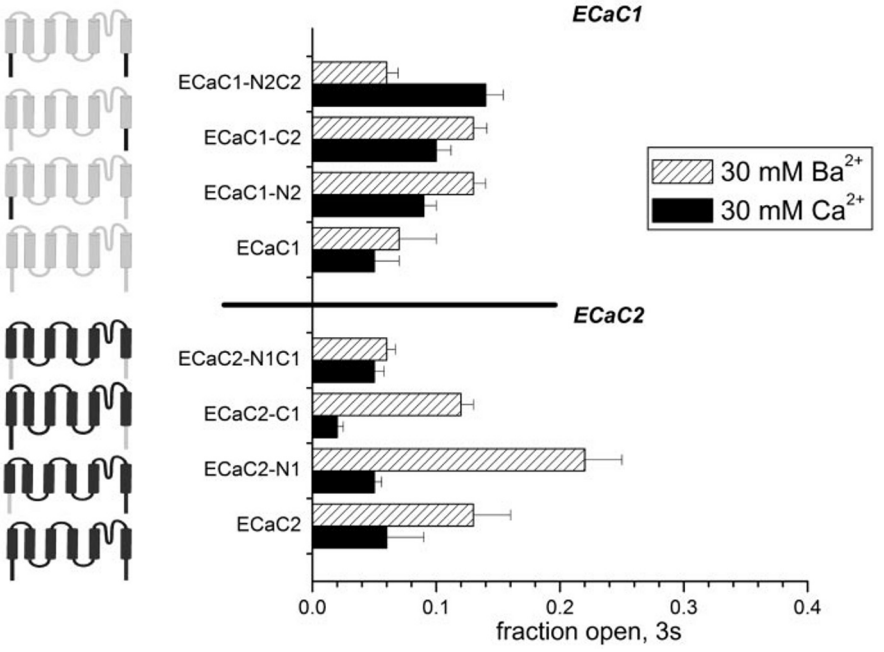

FIG. 5. **Summary of the inactivation properties of the chimeras.** The ratio of the current at the end of the 3-s step from +70 or +20 to −100 mV and the peak current are plotted against the respective chimera. The charge carrier is 30 mM Ca^{2+} (*solid bar*) or 30 mM Ba^{2+} (*striped bar*). Note that for all chimeras, the fraction of open channels is always <25%, indicating the substantial inactivation for all constructs.

ingly, the inactivation properties of the ECaC2 channel were drastically affected by substitution of its first intracellular loop with that of ECaC1 (Fig. 6). *Panel A* shows the main kinetic features of ECaC2 including fast initial inactivation, delayed inactivation with Ba^{2+} as the charge carrier, dramatic differences in the time to 10% inactivation between Ca^{2+} and Ba^{2+} currents, and a smaller current density of Ba^{2+} compared with the Ca^{2+} currents. The inactivation of both Ca^{2+} and Ba^{2+} currents was delayed in the loop1 ECaC2/$ICL1_{ECac1}$ chimera (Fig. 6, *B* and *C*). In addition, the fraction of channels inactivated at the end of the 3-s pulse was much less in ECaC2− compared with wild-type ECaC2 (Fig. 6*D*), indicating a defect of ECaC2 inactivation in this chimeric protein. The times to 10% inactivation were 929 ± 150 ms (n = 11) for Ca^{2+} and 2878 ± 40 ms (n = 8) for Ba^{2+}. In this analysis, the $t_{10\%}$ of the current that did not inactivate at all was set at 3 s, which is identical to the step duration. Thus, these quantitative data even represent an underestimation. The ratio between Ba^{2+} and Ca^{2+} current, I_{Ba}/I_{Ca}, was 0.36 ± 0.03 (n = 9, same cells), reflecting the ECaC2 phenotype. Similar results were obtained with 10 mM Ba^{2+} and Ca^{2+} as the charge carrier (data not shown, n = 12). Whether the opposite chimera, the first intracellular loop of ECaC2, $ICL1_{ECaC2}$, was introduced in ECaC1 (chimera ECaC1/$ICL1_{ECaC2}$), no dramatic changes were observed, although it displayed some features of the ECaC2 phenotype. Fig. 6*E* showed the kinetic behavior of this chimera. In contrast to wild-type ECaC1, the initial inactivation was significantly accelerated, *e.g.* from 112 ± 14 ms (n = 41) to 15 ± 3 ms (n = 9) for ECaC1/$ICL1_{ECaC2}$ (Fig. 6*F*). This value is much closer to ECaC2 (45 ± 5 ms, n = 24). Also in contrast to ECaC1, which does not strongly differentiate during the initial phase of inactivation between Ca^{2+} and Ba^{2+}, the ECaC1/$ICL1_{ECaC2}$ chimera has now a strikingly delayed time to 10% inactivation for Ba^{2+} as compared with Ca^{2+} (130 ± 25 ms, n = 8). The ratio between both times, $t_{10\%,Ca}/t_{10\%,Ba}$ was 0.18 ± 0.05, which was closer to the ECaC2 than to the ECaC1 phenotype. In addition, the ratio between the peak Ba^{2+} and Ca^{2+} currents, I_{Ba}/I_{Ca} was 0.47 ± 0.06, which is intermediate between the ECaC1 and ECaC2 phenotypes. The fraction of channels, which are open at the end of the 3-s step, was dramatically changed in the ECaC2/$ICL1_{ECaC1}$ chimera. However, the same change from ECaC2 to ECaC1 resulted again in the ECaC2 phenotype. The inactivation of the Ca^{2+} currents was nearly complete in both ECaC1 and ECaC2 (0.05 ± 0.02, n = 12, and 0.06 ± 0.03, n = 10). The inactivation of Ba^{2+} currents through ECaC2 was diminished as compared with ECaC1 (0.13 ± 0.03, n = 10, for ECaC2 and 0.07 ± 0.01, n = 10, for ECaC1). Similar data were measured for the ECaC1/$ICL1_{ECaC2}$ chimera, *e.g.* 0.11 ± 0.03 (n = 8) for Ba^{2+} and 0.030 ± 0.004 (n = 9) for Ca^{2+}. Thus, the kinetic behavior of this chimera further supports the essential role of the intracellular linker between TM2 and TM3 as a critical determinant of the kinetic behavior of the ECaC channels.

To identify the amino acid residues, which might be crucial for this dramatic change in phenotype, we have exchanged the divergent residues in TM2-TM3 of ECaC2 by the corresponding amino acids from the TM2-TM3 loop in ECaC1, *i.e.* L409V, V411A, T412S, and F414Y (Fig. 7). The effects of swapping the entire TM2-TM3 loop are depicted at the *top rows* of the *four panels*. The mutations at positions 409, 411, and 412 cause a significant delay of the initial decay of the Ca^{2+} current and a more pronounced prolongation of the inactivation of the Ba^{2+} current. These mutations resulted in a highly significant decrease of inactivation assessed from the ratio between the current at the end of the pulse and the peak current. An exchange of Phe-414 into a tyrosine had no effect. These data indicate that the N-terminal part of this intracellular linker is critically involved in controlling ECaC2 inactivation.

DISCUSSION

This study demonstrates that the intracellular loop between TM2 and TM3, particularly Leu-409, Val-411, and Thr-412, determines the initial rapid inactivation kinetics of ECaC1 and ECaC2, whereas the cytoplasmic N- and C-terminal tails do not contribute significantly.

Voltage-operated Ca^{2+} channels contain in the N and C termini major determinants of the inactivation process (17–23). Likewise, the N and C termini of the ECaCs contain many putative regulatory domains including protein kinase C and calmodulin-activating kinase phosphorylation sites, postsynaptic density protein, Disc large tumor suppressor, *Zonula occludens* protein motifs, and ankyrin repeats (2). It has been recently shown that the human isoform CaT-L is highly homologous to ECaC2 and inactivates in a Ca^{2+}-dependent

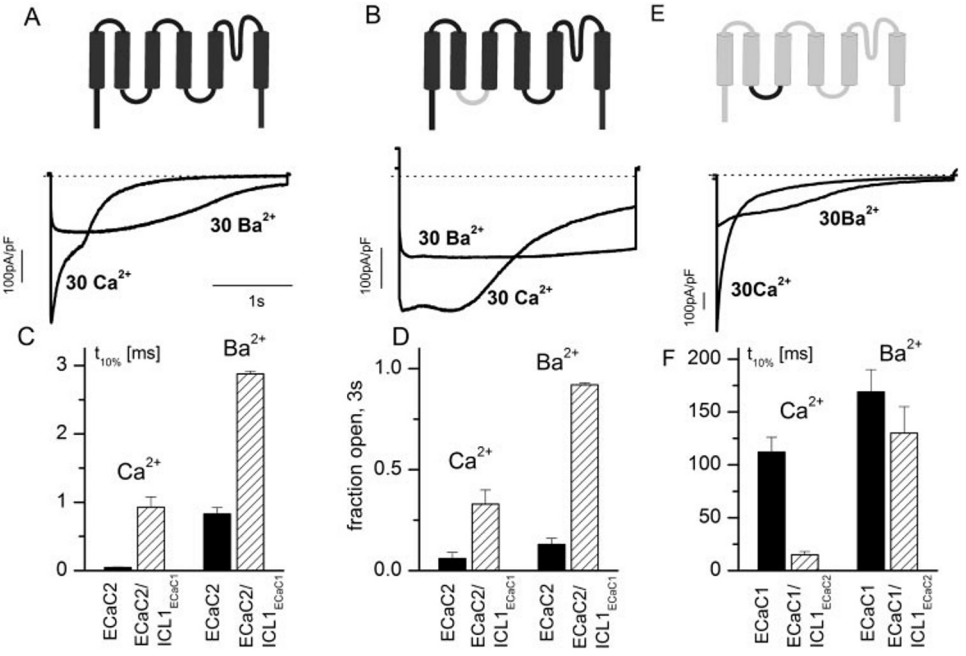

FIG. 6. **Inactivation properties of chimeras in which the intracellular loop between the transmembrane domains 2 and 3 in ECaC2 was replaced by the corresponding loop of ECaC1.** *A*, currents through the ECaC2 wild type. Conditions are the same as in Fig. 1. *B*, currents through the chimera ECaC2/$ICL1_{ECaC1}$ in which the intracellular loop between transmembrane domains 2 and 3 of ECaC2 was exchanged by the respective intracellular loop of ECaC1 ($ICL1_{ECaC1}$). *C*, summary of the time to 10% decay ($t_{10\%}$) for wild-type ECaC2 and the ECaC2/$ICL1_{ECaC1}$ chimera. *D*, pooled data comparing the fraction of inactivated channels after 3-s hyperpolarization to −100 mV from a holding potential of +70 mV. Note that the degree of inactivation was dramatically reduced for the chimeras for both Ca^{2+} and Ba^{2+} as the charge carrier. *E*, currents through the chimera ECaC1/$ICL1_{ECaC2}$ in which the intracellular loop between transmembrane domains TM2 and TM3 of ECaC1 was exchanged by the respective intracellular loop of ECaC2. *F*, summary of the time to 10% decay ($t_{10\%}$) for wild-type ECaC1 and the ECaC1/$ICL1_{ECaC2}$ chimera. Note the fast initial inactivation and the large difference between Ca^{2+} and Ba^{2+} for the chimera but not for wild-type ECaC1.

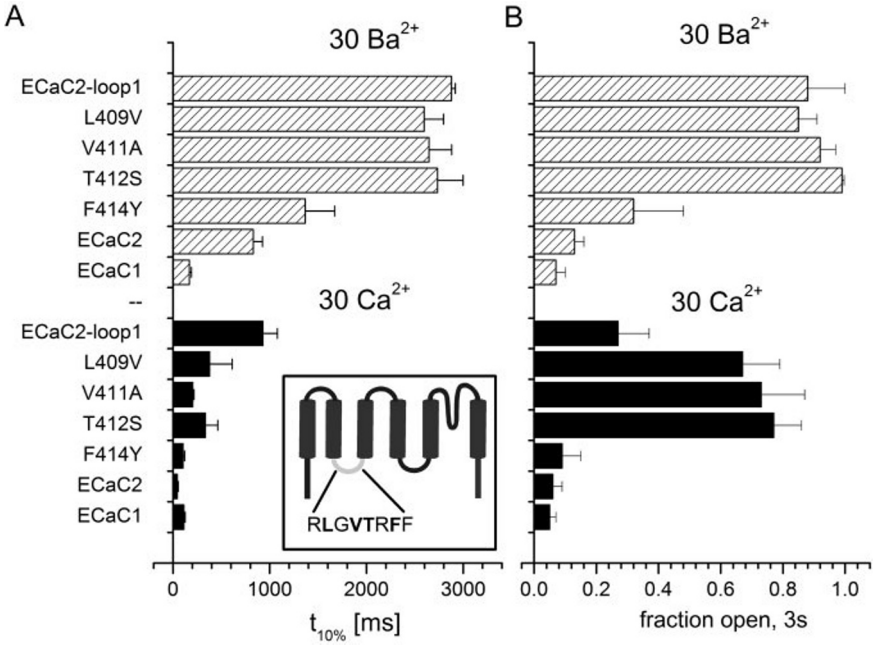

FIG. 7. **Inactivation properties of mutations in the TM2-TM3 loop of ECaC2.** *A*, pooled data for the fast decay of the current during the hyperpolarizing step to −100 mV for Ca^{2+} and Ba^{2+} as the charge carrier. The tested mutants are indicated at the *left*. *B*, degree of inactivation measured as the fraction of open channels at the end of the 3-s step (I_{3s}/I_{peak}). Note the dramatic defect of inactivation for the mutants at positions 409, 411, and 412 but not 414.

manner via a multiphasic process. This process is characterized by a rapid Ca^{2+}-dependent phase followed by a Ca^{2+}-CaM-dependent phase (24). The calmodulin-dependent inactivation can be counteracted by the phosphorylation of a protein kinase C site in the C terminus (24). However, the proposed calmodulin binding site in human CaT-L is not conserved, and also the protein kinase C site, which counteracts Ca^{2+}-dependent inactivation in CaT-L, is not present in ECaC1. Therefore, the swapping of the C termini of both ECaC channels could further evaluate such a mechanism. The cytoplasmic tails of ECaC1 and ECaC2 were exchanged, and the chimeric proteins expressed in HEK 293 cells were studied by patch clamp analysis. Surprisingly, the swapping of the entire intracellular N and C termini did not basically alter the inactivation kinetics of ECaC1 and ECaC2. Of note, Suzuki *et al.* (25) demonstrated that in the C terminus, the Q579H mutation in ECaC1 and the corresponding H587Q mutation in ECaC2 play a role in the inactivation process. However, in this latter study, the inactivation process was not studied in detail, and the information on the fast and subsequent slower inactivation process is lacking.

However, this study indicates that the cytoplasmic tails of ECaC1 and ECaC2 are not responsible for the difference in inactivation behavior of both channels.

A detailed comparison of the intracellular loops of ECaC1 and ECaC2 demonstrated that the domain between TM3 and TM4 is identical, whereas the loop between TM2 and TM3 contains four conserved amino acid differences (26). Chimeras were constructed in which the discriminating TM2-TM3 loop was exchanged. A subsequent electrophysiological analysis demonstrated that the characteristic fast inactivation of the ECaC2 current was absent in the ECaC2/ICL11 chimera and therefore mimicked the inactivation kinetics of ECaC1. The point mutations of the discriminating four amino acids revealed that Leu-409, Thr-412, and to a lesser extent Val-411 but not Phe-414 convey the molecular determinants of the fast inactivation process occurring in ECaC2. Importantly, this observation is further substantiated by the finding that transferring the ECaC2 TM2-TM3 linker to ECaC1 resulted in a shift of the kinetic phenotype of ECaC1 toward ECaC2. Especially, the inactivation of ECaC1 is accelerated, and the kinetic discrimination between Ca^{2+} and Ba^{2+} is accentuated. Interestingly, this critical motif is not present in other channel proteins and does not resemble the classical calmodulin-binding domain.

Interestingly, we have identified a short stretch of amino acids that is involved in the fast inactivation of ECaC2 when Ca^{2+} is the charge carrier. This situation is similar to Ca^{2+}-dependent inactivation of L-type α1C Ca^{2+} channels (27–29). In the study by Pitt *et al.* (29), it has been shown that Ca^{2+}-dependent inactivation requires the tethering of the Ca^{2+} sensor calmodulin to an effector region, which is supported by other stretches of amino acids. These stretches contain putative calmodulin-binding sequences. It is intriguing to speculate a similar role for the linker identified here. This linker is a critical motif, which is not present in other channel proteins. It does not resemble the classical calmodulin-binding domain but might contain a new calmodulin binding sequence or another inactivation mechanism, including interaction with another Ca^{2+} sensor, could be operative.

Another distinctive feature of both Ca^{2+} channels is that the ratio of Ba^{2+} and Ca^{2+} currents, I_{Ba}/I_{Ca}, through both channels is different (8), *e.g.* the ratio is significantly larger for ECaC1 than for ECaC2. This ratio may result from a smaller single channel conductance for Ba^{2+} than for Ca^{2+} for ECaC2 in comparison with ECaC1 or a decreased open probability of ECaC2 if Ba^{2+} is the charge carrier. This feature is again conserved for all chimeras including the loop chimera. The current ratio for all chimeras with the ECaC1 core was in a range between 0.69 and 1.15, whereas for all chimeras with the ECaC2 core, the ratio scattered between 0.39 and 0.56. This feature is also not changed by the translocation of the first intracellular linker and the mutations within this linker. This conserved behavior indicates that the mechanism by which both channels differentially discriminate between Ba^{2+} and Ca^{2+} is not located in the swapped domains and rather may be related to other region of the channels including the pore.

In conclusion, the present observations suggest that the residues Leu-409, Val-411, and Thr-412 present in the intracellular loop between TM2 and TM3 determine the fast inactivation of ECaC2. The ECaC2 residues may form part of an inactivation gate receptor region, and the definition of the state-dependent events may elucidate the molecular interactions important for gating transitions among closed, open, and inactivated states of the epithelial Ca^{2+} channel.

Acknowledgments—M. Crabbé, M. Schuermans, and A. Janssens are acknowledged for cell culture work.

REFERENCES

1. Harteneck, C., Plant, T. D., and Schultz, G. (2000) *Trends Neurosci.* **23,** 159–166
2. Hoenderop, J. G., van der Kemp, A. W., Hartog, A., van de Graaf, S. F., van Os, C. H., Willems, P. H., and Bindels, R. J. (1999) *J. Biol. Chem.* **274,** 8375–8378
3. Peng, J. B., Chen, X. Z., Berger, U. V., Vassilev, P. M., Tsukaguchi, H., Brown, E. M., and Hediger, M. A. (1999) *J. Biol. Chem.* **274,** 22739–22746
4. Nilius, B., Vennekens, R., Prenen, J., Hoenderop, J. G., Droogmans, G., and Bindels, R. J. (2001) *J. Biol. Chem.* **276,** 1020–1025
5. Müller, D., Hoenderop, J. G., Merkx, G. F., van Os, C. H., and Bindels, R. J. (2000) *Biochem. Biophys. Res. Commun.* **275,** 47–52
6. Müller, D., Hoenderop, J. G., Meij, I. C., van den Heuvel, L. P., Knoers, N. V., den Hollander, A. I., Eggert, P., Garcia-Nieto, V., Claverie-Martin, F., and Bindels, R. J. (2000) *Genomics* **67,** 48–53
7. Weber, K., Erben, R. G., Rump, A., and Adamski, J. (2001) *Biochem. Biophys. Res. Commun.* **289,** 1287–1294
8. Hoenderop, J. G. J., Vennekens, R., Müller, D., Prenen, J., Droogmans, G., Bindels, R. J. M., and Nilius, B. (2001) *J. Physiol. (Lond.)* **537,** 747–761
9. Hoenderop, J. G., Hartog, A., Stuiver, M., Doucet, A., Willems, P. H., and Bindels, R. J. (2000) *J. Am. Soc. Nephrol.* **11,** 1171–1178
10. Nilius, B., Vennekens, R., Prenen, J., Hoenderop, J. G., Bindels, R. J., and Droogmans, G. (2000) *J. Physiol. (Lond.)* **527,** 239–248
11. Nilius, B., Prenen, J., Vennekens, R., Hoenderop, J. G., Bindels, R. J., and Droogmans, G. (2001) *Cell Calcium* **29,** 417–428
12. Vennekens, R., Hoenderop, J. G., Prenen, J., Stuiver, M., Willems, P. H., Droogmans, G., Nilius, B., and Bindels, R. J. (2000) *J. Biol. Chem.* **275,** 3963–3969
13. Vennekens, R., Prenen, J., Hoenderop, J. G., Bindels, R. J., Droogmans, G., and Nilius, B. (2001) *J. Physiol. (Lond.)* **530,** 183–191
14. Yue, L., Peng, J. B., Hediger, M. A., and Clapham, D. E. (2001) *Nature* **410,** 705–709
15. Voets, T., Prenen, J., Fleig, A., Vennekens, R., Watanabe, H., Hoenderop, J. G. J., Bindels, R. J. M., Droogmans, G., Penner, R., and Nilius, B. (2001) *J. Biol. Chem.* **276,** 47767–47770
16. Nilius, B., Prenen, J., Vennekens, R., Hoenderop, J. G. J., Bindels, R. J. M., and Droogmans, G. (2001) *Br. J. Pharmacol.* **134,** 453–462
17. Kepplinger, K. J., Kahr, H., Forstner, G., Sonnleitner, M., Schindler, H., Schmidt, T., Groschner, K., Soldatov, N. M., and Romanin, C. (2000) *FEBS Lett.* **477,** 161–169
18. Soldatov, N. M., Zhenochin, S., AlBanna, B., Abernethy, D. R., and Morad, M. (2000) *J. Membr. Biol.* **177,** 129–135
19. Soldatov, N. M., Zühlke, R. D., Bouron, A., and Reuter, H. (1997) *J. Biol. Chem.* **272,** 3560–3566
20. Marksteiner, R., Schurr, P., Berjukow, S., Margreiter, E., Perez Reyes, E., and Hering, S. (2001) *J. Physiol. (Lond.)* **537,** 27–34
21. Berjukow, S., Marksteiner, R., Sokolov, S., Weiss, R. G., Margreiter, E., and Hering, S. (2001) *J. Biol. Chem.* **276,** 17076–17082
22. Lee, A., Wong, S. T., Gallagher, D., Li, B., Storm, D. R., Scheuer, T., and Catterall, W. A. (1999) *Nature* **399,** 155–159
23. Staes, M., Talavera, K., Klugbauer, N., Prenen, J., Lacinova, L., Droogmans, G., Hofmann, F., and Nilius, B. (2001) *J. Physiol. (Lond.)* **530,** 35–45
24. Niemeyer, B. A., Bergs, C., Wissenbach, U., Flockerzi, V., and Trost, C. (2001) *Proc. Natl. Acad. Sci. U. S. A.* **98,** 3600–3605
25. Suzuki, M., Ishibashi, K., Ooki, G., Tsuruoka, S., and Imai, M. (2000) *Biochem. Biophys. Res. Commun.* **274,** 344–349
26. Hoenderop, J. G. J., Müller, D., Suzuki, M., van Os, C. H., and Bindels, R. J. M. (2000) *Curr. Opin. Nephrol. Hypertens.* **9,** 335–340
27. Zühlke, R. D., Pitt, G. S., Deisseroth, K., Tsien, R. W., and Reuter, H. (1999) *Nature* **399,** 159–162
28. Zühlke, R. D., Pitt, G. S., Tsien, R. W., and Reuter, H. (2000) *J. Biol. Chem.* **275,** 21121–21129
29. Pitt, G. S., Zühlke, R. D., Hudmon, A., Schulman, H., Reuter, H., and Tsien, R. W. (2001) *J. Biol. Chem.* **276,** 30794–30802